The channel architecture of aquaporin 0 at a 2.2-Å resolution

William E. C. Harries, David Akhavan, Larry J. W. Miercke, Shahram Khademi, and Robert M. Stroud*

Macromolecular Structure Group, Department of Biochemistry and Biophysics, University of California, S-412C Genentech Hall, 600 16th Street, San Francisco, CA 94143-2240

Communicated by James A. Wells, Sunesis Pharmaceuticals, Inc., South San Francisco, CA, August 10, 2004 (received for review June 10, 2004)

We determined the x-ray structure of bovine aquaporin 0 (AQP0) to a resolution of 2.2 Å. The structure of this eukaryotic, integral membrane protein suggests that the selectivity of AQP0 for water transport is based on the identity and location of signature amino acid residues that are hallmarks of the water-selective arm of the AQP family of proteins. Furthermore, the channel lumen is narrowed only by two, quasi-2-fold related tyrosine side chains that might account for reduced water conductance relative to other AQPs. The channel is functionally open to the passage of water because there are eight discreet water molecules within the channel. Comparison of this structure with the recent electron-diffraction structure of the junctional form of sheep AQP0 at pH 6.0 that was interpreted as closed shows no global change in the structure of AQP0 and only small changes in side-chain positions. We observed no structural change to the channel or the molecule as a whole at pH 10, which could be interpreted as the postulated pH-gating mechanism of AQP0-mediated water transport at pH >6.5. Contrary to the electron-diffraction structure, the comparison shows no evidence of channel gating induced by association of the extracellular domains of AQP0 at pH 6.0. Our structure aids the analysis of the interaction of the extracellular domains and the possibility of a cell–cell adhesion role for AQP0. In addition, our structure illustrates the basis for formation of certain types of cataracts that are the result of mutations.

The vertebrate ocular lens is a remarkably transparent and avascular tissue that acts basically as a syncytium of differentiated epithelial cells, called fiber cells. These cells are thin and highly elongated, and they are essentially a plasma membrane-enclosed sack filled with transparent crystallin proteins. The lens is covered on the surface of its anterior hemisphere with a layer of simple squamous epithelial cells and an acellular capsule that encloses the entire lens. The lack of vascular-supply structures and any identifiable active transport systems in the fiber cell mass means that diffusional pathways are of paramount importance to the establishment and maintenance of lens homeostasis and transparency. The transparency of the lens, together with its ability to undergo dynamic shape changes during accommodation, provides for a clear and accurate image of the world to be projected onto the retina. The transparent nature of the lens is contingent on several crucial features that permit light to pass through with a minimum of light scattering. These features are (*i*) the maintenance of a highly ordered molecular structure of the crystallin proteins; (*ii*) terminally differentiated fiber cells containing very few organelles; and (*iii*) intracellular and intercellular spaces being kept smaller than the wavelength of ambient light (1–3).

It is intriguing to understand the cellular and molecular basis for the maintenance of lens transparency, as well as the loss of lens transparency due to pathological and injury-induced conditions. Lens physiology has implicated water as one culprit that is often responsible for the disruption of crystallin molecule transparency; the movement of excess water across the lens fiber cell membrane into the fiber cell induces the hydration of crystallin proteins that disrupts their transparent molecular structure. The major integral membrane protein of the lens fiber cell, aquaporin 0 (AQP0), is thought to be a key player in maintaining a healthy functional lens by regulating water permeation across the fiber cell plasma membrane. Bovine AQP0 (bAQP0) is composed of 263 amino acids and accounts for >60% of the fiber cell plasma membrane protein complement (4–6). The measured functions have been controversial. AQP0 was initially postulated to be a gap-junction protein that forms voltage-dependent, nonspecific channels with the ability to transport substances as large as 1,500 Da, and it was then postulated to be a cell–cell adhesion molecule. The genetic sequence of AQP0 identified it as a member of the AQP, rather than the connexin, family (7) and thereby predicted its role in the establishment and maintenance of lens homeostasis (8). However, measured water transport is 15-fold lower than for AQP1 at pH 6.5 and is reduced to 46-fold lower than AQP1 at pH 7.5 (9).

To address the roles of AQP0 and, in particular, its roles in water transport and cell adhesion in the lens, we determined the 3D structure of bovine AQP0 to a resolution of 2.2 Å. This structure helps to explain the observed water transport and its regulation through these channels. The structure also provides insight into the possible role that AQP0 plays in lens accommodation through its cell-adhesion activity, as well as the effect of cataract-inducing mutations on the structure of AQP0 and the transparency of the lens as a whole.

Since the submission of this manuscript, an electron diffraction-derived structure of sheep AQP0 (sAQP0) at a resolution of 3.0 × 3.5 Å was published by Walz and coworkers (10). Their structure was for a junctional form of doubled membranes at pH 6.0, used 2D crystals of sAQP0, and does not reveal any water molecules. Overall, the x-ray and electron-diffraction structures are remarkably similar to an α-carbon rms deviation of 1.12 Å. Residues 6–239 were common to both structures. The only four residues that are different between bAQP0 and sAQP0 sequences (bAQP0 numbering) are C14F, S20T, M90V, and S240T (S240T does not appear in either structure). The comparisons between the two structures instruct as to differences that may be caused by the junctional molecular contact vs. the isolated tetramers, by the differences in pH, or by any difference between membrane- bound and detergent-solubilized AQP0, and they could reveal differences related to any of the postulated gating mechanisms that depend on junctional contact or pH effects.

The pH-gating mechanism proposed by Nemeth-Cahalan and Hall (11) and Nemeth-Cahalan *et al.* (12) by their criteria shows AQP0 maximally conducting at pH ≈6.5 and conducting 3.4-fold less at pH ≈8.5 (however, any pH-dependent gating has been challenged; ref. 13). For Walz and coworkers (10), sAQP0 crystals were formed at pH 6.0, whereas our bAQP0 crystals were formed at pH 10.0. The channel would be expected to be closed if any pH gating were to persist at pH >8.5, and thus, the two structures could illustrate any pH-dependent structural

BIOCHEMISTRY

Abbreviations: AQP(*n*), aquaporin (*n*); bAQP*n*, bovine AQP*n*; sAQP0, sheep AQP0; OG, octylglucopyranoside; NPA, Asn-Pro-Ala sequence.

Data deposition: The atomic coordinates have been deposited in the Protein Data Bank, www.pdb.org (PDB ID code 1TM8).

*To whom correspondence should be addressed. E-mail: stroud@msg.ucsf.edu.

changes associated with closure at high pH (or any pH-dependent structural changes at all). Our structure seems to be functionally open, and thus, there is little evidence in the structure to support blockade in a static sense at pH 10.

In contrast, the "double-layer" structure is thought to be in a closed form (10), even though it is found to be mostly open in a single membrane at pH 6.5. The x-ray structure ($P42_12$) does not have individual AQP0 molecules or tetramers associating through their extracellular surfaces, whereas the electron diffraction double-layered structure (P422) has direct close approximation of the extracellular domains in a conformation that may represent one *in vivo* form. Therefore, any changes in the channel architecture that are due to extracellular-domain interactions should also be apparent.

Materials and Methods

AQP0 Purification, Characterization, and Crystallization. Lenses were removed from fresh bovine eyes (Harris Ranch Beef, Selma, CA), rinsed in lens buffer (0.5 M NaCl/20 mM Tris, pH 8.0/1 mM EDTA/0.5 mM PMSF), and decapsulated. The lenses were homogenized, stirred overnight, and washed five times by centrifugation at 125,000 × *g* for 1 h. Even though stripping the membranes with urea and alkaline buffer (14) removes most membrane protein contaminants (15); this treatment induced AQPO oligomerization upon purification (W.E.C.H., L.J.W.M., and D.A., unpublished data) and, thus, was not performed. AQP0 was purified according to ref. 16 with the following changes: 300 mM octylglucopyranoside (OG) was used for solubilization, followed by cation exchange at pH 9.0 (20 mM bicine/40 mM OG/1M NaCl elution) and size-exclusion (TSK) by using 10 mM *n*-nonyl-β-D-glucoside (NG) at pH 7.0 (20 mM Hepes/0.4 M NaCl). Before crystallization, the second eluted TSK peak was concentrated to 5–10 mg/ml (stirred-cell concentrator; Amicon; YM-30 membrane) and dialyzed for 3 days against 10 mM bicine, pH 9.0/10 mM NG/50 mM NaCl in a 100-KDa cut-off bag. The mass of purified bAQP0 was measured to within 1 Da of the mass calculated from the amino acid sequence by using matrix-assisted laser desorption ionization–time-of-flight MS and a sinapinic acid matrix. The radius of hydration and molar mass of bAQP0/OG protein–detergent complex were measured by combination of UV absorbance, viscosity, refractive index, and light scattering, and they were found to be 4.83 nm and 187,857 Da, respectively (Tetra-Detector analysis coupled with a TSK3000SW size-exclusion column; Viscotek, Houston). Therefore, the protein is tetrameric in solution and contains 0.66 g of OG per g of protein, or 256 mol of OG per mol of AQP0 tetramer, identical to that found by using analytical centrifugation and the anthrone method (17).

Crystallization Methods. Sitting drops were set up in a vapor-diffusion chamber by using equal volumes of protein solution and well solution (usually 2 μl of each solution) at room temperature. The well solution was 30% polyethylene glycol 1K/20 mM glycine, pH 10.0/50 mM NaCl. Although many conditions gave crystals, only one condition gave high-resolution diffracting crystals, and these crystals first appeared over the course of several months and "matured" over 1 year of incubation before the crystals diffracted to 2.20 Å. These crystals were regular tetragonal prisms of 100–200 μm in length, and they were uniaxially birefringent under polarized light.

Data Collection. Crystals were looped out of their drops and frozen by rapid immersion into liquid nitrogen. Data were collected at Beamline 8.3.1 at the Advanced Light Source (ALS) at the Lawrence Berkeley National Laboratory (Berkeley, CA). The crystals were mounted onto the synchrotron goniometer and kept at approximately −100 K in a nitrogen cryostream. Four data sets were taken from different nonoverlapping areas of one crystal. The four data sets were processed by using by DENZO (18) and MOSFLM (19). The data used for refinement were the output of DENZO/SCALEPACK. The initial phase and solution was determined by molecular replacement using the 2.2-Å structure of bAQP1 as the search model. All subsequent refinement was carried out by using CNS (20) and MOLOC (21).

Table 1. Crystallographic statistics of 2.2-Å data

Data collection statistics	
Wavelength, Å	1.0
Resolution, Å	30.0–2.2
Total reflections	340,485
Unique reflections	14,682
Completeness, % (last shell)*	89.5 (49.2)
R_{sym}, % (last shell)	4.1 (50.4)
I/σ (last shell)	28.0 (2.6)
Refinement statistics	
Space group	$P42_12$
Unit cell dimensions	$a = 110.5$, $c = 53.4$
Resolution, Å	30.0–2.2
R_{cryst}, %	24.8
R_{free}, %	27.1
rms deviation bonds, Å	0.006
rms deviation angles, Å	1.207
Nonhydrogen protein atoms	1,803
Nonhydrogen heteroatoms	42
Solvent molecules	181
Average B-factors, Å^2	54.7
B values from Wilson Plot, Å^2	25.7

Data were collected at ALS Beamline 8.3.1 with an 2 × 2 charge-coupled device detector (ADSC, Poway, CA), integrated, and scaled with MOSFLM/SCALA and DENZO/SCALEPACK (18, 20). Phasing calculations were carried out by using molecular replacement with bAQP1 as the model, and CNS was used for the data refinement. The rms deviation from ideal geometry is given. $R_{sym} = \Sigma_{hkl}\Sigma_i|I_{hkl,i} - \langle I_{hkl,i}\rangle|/\Sigma_{hkl}\Sigma_i|I_{hkl,i}|$, where $\langle I_{hkl,i}\rangle$ is the average intensity of the multiple hkl observations for symmetry-related reflections. $R_{cryst} = \Sigma|F_{obs} - F_{calc}|\Sigma F_{obs}$, where F_{obs} and F_{calc} are observed and calculated structure factors, respectively, R_{free} is calculated from a randomly chosen 10% of reflections, and R_{cryst} is calculated over the remaining 90% of reflections.
*Last-shell resolution, 2.28–2.20.

Supporting Information. See *Supporting Methods* and Figs. 6–10, which are published as supporting information on the PNAS web site, for more details.

Results and Discussion

The Structure of bAQP0. The x-ray diffraction data collected from three separate nonoverlapping regions of one crystal were merged (Table 1). During purification and crystallization, bAQP0 remains a tetramer. Its 4-fold axis in the crystal is aligned with the *c* axis, and thus, the plane of the membrane would lie perpendicular to the *c* axis. In the plane of the membrane, the tetramer is ≈60 Å wide (≈74 Å, corner to corner) and ≈53 Å tall. Each bAQP0 monomer is ≈35 Å in diameter and contains one channel at its center that is oriented parallel to the 4-fold axis of the tetramer, as in other AQPs (Fig. 1) (9, 22, 23). Note that four of the five 3D crystals and atomic-level structures of AQPs crystallize in different packing arrangements of the tetramers, as reflected in their different space groups. Thus, whereas the monomers form tetramers in the same manner, tetramers pack together differently, and the basis for forming a crystal is different in each case.

The structure starts with residue 6 and ends with residue 239, representing 88% of the molecule. Because the complete primary sequence of bAQP0 is intact as determined by MS, five

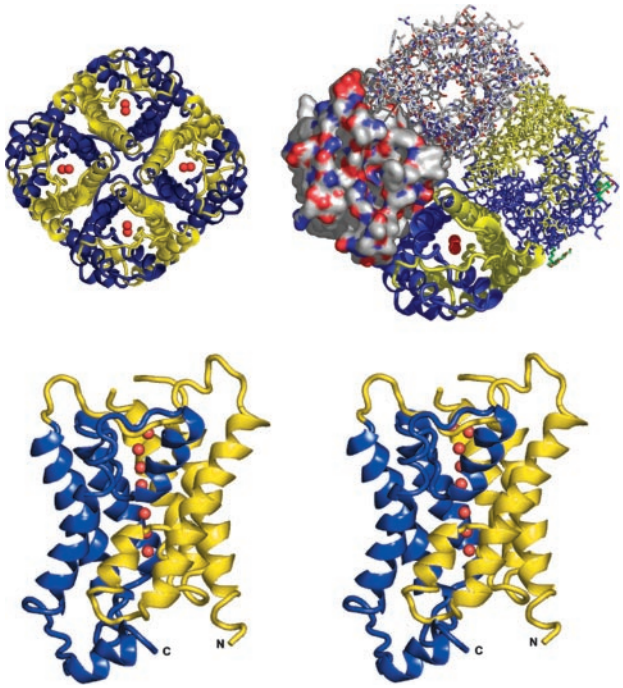

Fig. 1. Tetramer and monomer structure of bAQP0. (*Upper Left*) Cartoon of the bAQP0 tetramer looking down the *z* axis from the extracellular side of the protein. Yellow and blue indicate structures derived from each of the two gene-duplicated portions of the primary sequence. (*Upper Right*) Cartoon showing the same view as in *Upper Left*, with each monomer shown in a different representation. (*Lower*) Cartoon of an bAQP0 monomer in a side view, with the uppermost extracellular side in crossed eye stereo. All images were made with PYMOL (DeLano Scientific, San Carlos, CA).

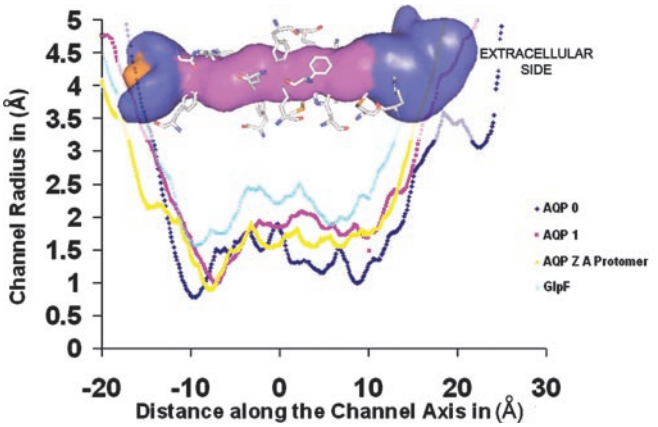

Fig. 3. Channel radius profile plot. Channel radius profiles of AQPs of known structure with corresponding structural elements are shown (22, 23). The AQPZ ''A'' protomer was used for radius calculations for AQPZ. The distance along the channel axis is calculated by using a point midway between the Asn-Pro-Ala sequences (NPAs) as the zero point. Radii were calculated with HOLE (39). Channel volume is shown in the background, with major channel-forming residues. The pink central region has a diameter of <2.5 Å, the blue region has a diameter of >2.5 Å and <10 Å. All images were made with PYMOL.

residues at the N terminus and 24 residues at the C terminus are not well ordered in the structure. The useful electron density ends at residue 239, and the N and C termini lie on the cytoplasmic side of the membrane.

The 28-Å-long, cylindrical bAQP0 channel is flanked by shallow vestibules on each end (Fig. 2). Starting from the extracellular side, the vestibule narrows to a diameter of <10 Å between residues Asn-115, Thr-120, and His-34. His-34 is oriented into the center line of the channel and is responsible for most of the narrowing of the vestibule. The channel narrows a diameter of 1.99 Å at residues Phe-48(Trp-48), His-172(Ile-190), Met-176(Gly-195), Ala-181(Phe-200), and Arg-187(206). In AQP1, AQPZ, and GlpF, this region is the narrowest region of the channel (Fig. 3) (9, 22, 23). Four backbone carbonyls of successive residues [Gly-180(Thr-198), Ala-181(Gly-199), Gly-182(Phe-200), and Met-183(Ala-201)] provide the canonical AQP hydrogen bond acceptors that align waters through the channel. The OD1 of Asn-119(Val-129), NH2 of Arg-187(Ala-205), and His-172(Ile-190) provide donor hydrogen bonds for the waters. These residues bind four ordered water molecules (Fig. 2 *Center*) and further orient the channel waters. Farther into the channel, the side chain of Tyr-23(Leu-21) is oriented directly toward the central axis of the channel and, with Phe-141(Leu-159), Leu-52(Val-52), and Leu-168(186), constricts the channel diameter to 2.5 Å. Just after the Tyr-23 constriction are Asn-68(68) and Asn-184(203) of the signature NPA–NPA motifs

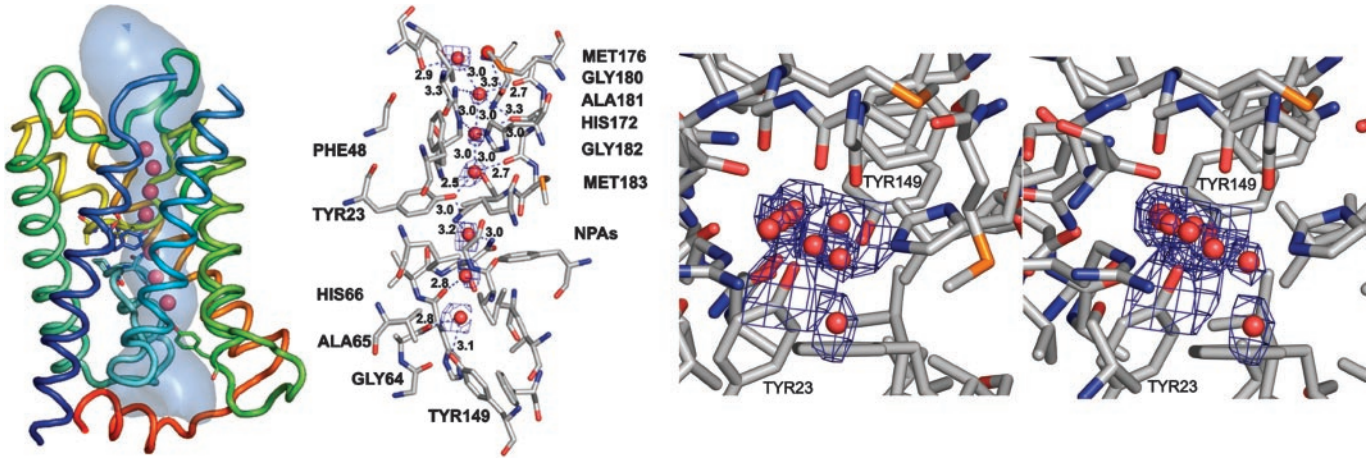

Fig. 2. Monomer channel views of bAQP0. (*Left*) Side view of the monomer and water molecules (red spheres) in the channel. The channel luminal surface is shown in light blue. Each helix is colored in order of the rainbow. (*Center*) Side view looking from the midmembrane plane toward the monomer channel residues and water molecules in the channel. Hydrogen bonds to the channel waters are shown as dotted lines. Electron density around waters is shown in a composite omit 2Fo–Fc map contoured at 0.5 σ for clarity. (*Right*) Stereo view from the extracellular side of the channel. Electron density around waters and Tyr-23 and Tyr-149 are contoured at 0.5 σ. All images were made with PYMOL.

that orient the key central water molecule that is responsible for preventing the reorientation that would be necessary for any proton conduction. On the cytoplasmic side of the NPAs, the line of backbone carbonyl oxygens resumes along one wall of the channel from Gly-64(64), Ala-65(65), His-66(66), and Gly-67(67), and it ends at Tyr-149(Thr-167). The line of eight backbone carbonyls and other channel-lining residues establishes a tight single-file pathway for water highlighted by the eight water molecules in the channel.

Tyr-149(Thr-149) points directly into the channel and, together with Val-56(Ile-56), Gly-64(64), His-66(66), and Phe-75(Leu-75), forms another constriction that is the narrowest region of the channel. It accepts a sphere with a maximum diameter of 1.5 Å (as determined by using the program HOLE; ref. 21). In AQP0, it serves as a cytoplasmic end of the narrow part of the channel. Continuing in toward the cytoplasmic side, the channel widens slightly to accept a sphere with an average diameter of 3 Å, which is significantly narrower than in other AQP structures (AQP1, 3.5–4.0 Å; GlpF, 4.0–5.0 Å) (22, 23). The two residues Tyr-23(Leu-21) and Tyr-149(Thr-149) are in quasi-2-fold related positions evoked by gene duplication, and in the other AQPs, Tyr-23(Leu-21) is either a phenylalanine or a leucine and Tyr-149(Thr-149) is either a threonine or leucine.

Water Conductance. An apparent paradox is that the lens fiber cell must keep its interior relatively dry to maintain crystallin protein transparency, but it invests a significant percentage of its cellular resources to produce large amounts of AQP0, a member of the water channel family. Why should the fiber cell invest so much synthetic energy to produce a protein that could seemingly compromise crystallin transparency? Clearly, the lens requires a basal level of water conductance for good health and the great longevity of the lens cells, most of which live for the entire lifespan of the organism. However, the fiber cell compensates for having an incredibly large number of these channels (≈60% by weight of all membrane proteins in the fiber-cell plasma membrane is AQP0) by having AQP0 conduct water very poorly. Thus, it ensures a uniform response to osmotic challenge in all areas of the cell surfaces of the tightly packed fiber cells throughout the lens and maintains homogeneous transparency throughout the lens.

Measurements of water conductance using oocyte and proteoliposome swelling demonstrate that AQP0 water permeability is 15- to 45-fold less than AQP1 (11, 24–29). Published water-permeability data have varied from 0- to 43-fold over conduction through lipids alone or through the membranes of oocytes injected with water. Unfortunately, comparisons between published conduction rates are difficult because they are generally relative conductances uncorrected for the number of conducting channels, and they are also difficult because of the variety of materials and methods used.

A question arises as to the channel dimensions required for passage of various permeants through the channel. Use of the minimum diameter of the permeant as a rough measure of the channel diameter required for passage, as well as the diameter of the largest sphere that will fit in the channel at the narrowest constriction of the channel, provides one criterion. The diameter of the channel calculated in this way for a static structure would suggest that both of our structures of AQP0 channel (d = 1.5 Å) and the Walz structures of AQP0 channel (d = 2.0 Å) are too narrow to permit the passage of water and other larger permeants, including glycerol and urea. Previous functional studies have shown significant measurable flux through AQP0 of all three of these substances, even though some of these results are questionable. However, if the channel were to have a noncircular profile, then the available cross-sectional area could be larger than the value implied by this calculation. Further, the channel diameter values calculated for bAQP0, AQP1, and AQPZ are also all smaller than the accepted value of 2.8 Å for the diameter of a single water molecule, yet all of these AQPs conduct water at close to the diffusion-limiting rate. Therefore, to test the possible accommodation of AQP0 to these substrates, we selected side-chain rotamers of constriction-region residues of our AQP0 structure that maximized channel diameter without any main chain movement. After extensive energy minimization and annealing, the resulting structures had stable rotamers that could enlarge the channel diameter to slightly >2.9 Å, which is more than large enough for water to pass. Additional circumstantial evidence of water transport is the presence of eight hydrogen-bonded water molecules in the channel (no waters are seen in the electron-diffraction structure). These waters are moderately well ordered, as reflected by their electron densities (Fig. 2 *Center*) and by their B factors, which are close to the average for the protein ($\langle B \rangle$ = 55) as follows: 57, 57, 54, 51, 48, 44, 41, and 38, from extracellular to intracellular in the channel. Thus, there is water throughout the channel pathway (Figs. 1 and 2).

The two channel-constricting tyrosines (Tyr-23 and Tyr-149) that are totally conserved in all known AQP0s, suggests the possibility of "kinetic limiting" (namely, if both tyrosines have to move out of the channel simultaneously to achieve high conductance, the probability of both of them allowing passage together is the product of the probabilities of each one individually).

Regulation of Water Conductance by pH, Ions, or Posttranslational Modification? Modulation by changes in pH or ion concentration have been suggested in the control of transport of water and possibly other substrates (10, 11, 13, 30–35) through AQP0. However, Boron and coworkers (13) argue against these effects and show zero dependence on pH or Ca^{2+}. His-40 has been suggested to be the residue that is responsible for the inhibitory effect of pH or Ca^{2+} on water transport rates (11–13). Therefore, Nemeth-Cahalan and Hall made mutations that changed His-40 to alanine, aspartate, or lysine, and they showed that treatment of oocytes expressing the mutants no longer displayed the pH-dependent closing as pH was raised to >6.5. Reaction of histidines in AQP0 with diethylpyrocarbonate (DEPC) removed pH dependence and actually increased water conductance (restored by histidine-specific reversal with hydroxylamine), adding support to the case that titration of histidines alters conductance (11, 12).

The comparison of the two structures (pH 10 vs. 6.0) brackets the range of observed pH dependence and, therefore, should reveal any structural consequences of His titration. The comparison shows no positional difference of His-40 in the extracellular vestibule, His-172 (which lies in the wall of the channel), or His-66 in the cytoplasmic vestibule (where it is the hydrogen bond acceptor from Thr-72). Because of their water-accessible position, one could expect the pK_a of His-40 and His-66 to be relatively normal and unlikely to be responsible for gating at higher pH without structural change that we do not see at pH 10 vs. 6. His-172 near the extracellular constriction region is hydrogen bond donor to the second water in the line of waters throughout the channel (see Fig. 4 *Lower Left*). Thus, all three histidines show no evidence of pH-dependent conformational change.

Posttranslational modifications have also been suggested in the regulation of AQP0 activity. Published evidence is again contradictory, perhaps because of the difficulty of measuring lower water conductance relative to lipid conductance. However, we find no evidence for any posttranslational modifications (by, for example, gylcosylation, deamidination of Asn-246, and phosphorylation) in our samples by MS of freshly prepared AQP0 or the x-ray structure after additional time and purification. PAGE gels stained for the presence of glycosylation were also negative. The lenses were taken from 1- to 2-year-old cattle in good health, so most age-related covalent additions, such as glycosylation and

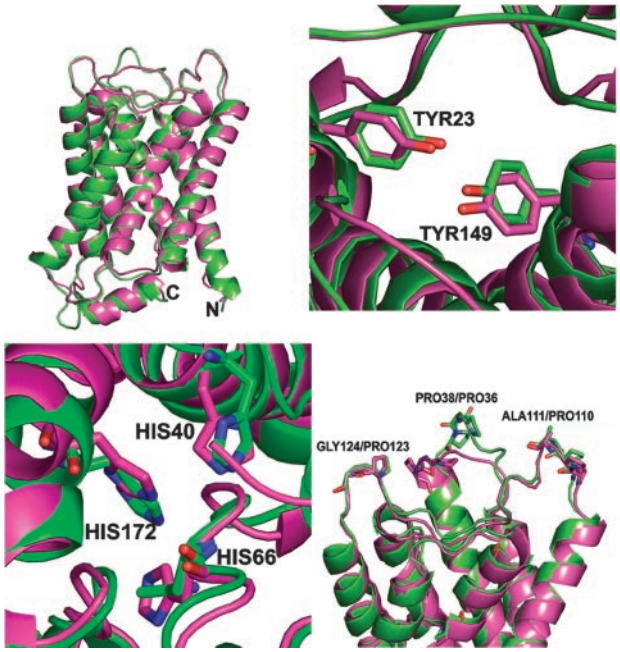

Fig. 4. Comparisons of the x-ray and electron crystal structures. (*Upper Left*) Structures overlaid with x-ray structure are shown in purple, and the electron-diffraction structure is shown in green. (*Upper Right*) View down the monomer channel *z* axis from the extracellular side showing the positions of Tyr-23 and Tyr-149. (*Lower Left*) View down the monomer channel *z* axis from the extracellular side showing the positions of the three histidines that are close to the channel and vestibules. (*Lower Right*) Side view. The extracellular residues involved in cell-to-cell contacts are highlighted and labeled.

phosphorylation to bAQP0, were minimized. Ser-235, Ser-243, and Ser-245 in the C-terminal chain have been implicated as regulatory phosphorylation sites in bAQP0 (30). Two of these residues are in the mobile C-terminal 24 amino acids (239–263) and are not represented by electron density in our structure of bAQP0.

Conformational Consequences of Junction Formation. Perhaps surprisingly, junction formation does not produce any significant difference in the degree of openness of the channel, or the loops that contribute to the junction or the structure of AQP0. The definition of probable error in each atom coordinate is a well defined function of resolution and data to parameter ratio for each structure, as elaborated by R.M.S. and Fauman (36). Any shift below the sum in quadrature of error in the two structures is by definition not detectable. The error in the x-ray coordinates is typically ≈0.2 Å.

Observing that the channel seemed to be more closed than in other AQPs, Walz and coworkers (10) had proposed several mechanisms that might alter the channel dimensions and, thus, constitute a gating mechanism evoked by junction formation of AQP0. In the comparison, we see that junctional formation does not produce any closure *per se*. Overlaying the two structures reveals no change in the constriction around Tyr-23 or Tyr-149, which are the most likely sites of any channel closure because of interactions of the associating extracellular domains (Fig. 4 *Upper Right*). Therefore, junction formation does not appear to lead to any physical closure of the channel.

Walz and coworkers (10) showed that loop C mediates most of the junction-forming interactions, and they suggest that it may be altered by the contact formation, suggesting that if this possibility were true, it could stabilize an alternate conformation of Arg-187 located in the central "selectivity filter" of the channel to contribute to channel closure (19). In our findings, there is essentially no difference in loop C, or the diameter of the channel, between the two structures, suggesting that it is not part of a switching mechanism. Also, Arg-187 makes two good hydrogen bonds from NH1 to the C═O of 187 and to C═O of Ala-117, which we find to be conserved throughout all AQPs. Because of a slight difference in placement of Arg-187, the electron-diffraction structure claims a hydrogen-bonded contact between the amidinium cation of Arg-187 and Asn-119; however, the geometry of this interaction is 90° from ideal and seems to be unlikely. Otherwise, there is no significant change in the conformations of Arg-187, Ala-117, and Asn-119. Thus, it is improbable that close approximation of adjacent extracellular domains acts as a gating mechanism by inducing distortion of the channel in this region either.

The most striking difference between the two AQP0 structures is the association between tetramers in the crystals. Our AQP0 tetramers have their cytoplasmic domains in contact with the extracellular domains of the adjacent tetramers along the 4-fold axis in space group $P42_12$. In the double-membrane structure the AQP tetramer extracellular domains of one layer face each other between parallel bilayers, an organization that is thought to mimic an *in situ* state in cell–cell association (10). The antipodal difference in association of tetramers seems to imply that the intermolecular forces between tetramers in the double layer are generally weak and assemble the double layer by using the avidity effect of many such weak interactions when tethered by 2D constraints in membranes.

Regarding whether the close apposition of AQP0 tetramers could form aligned, sealed cell–cell junctions, one asks whether the very close approximation of the extracellular domains of AQP0 tetramers closes off access to the channels from the extracellular environment. We answer no; there are several large gaps between the opposing extracellular domains of AQP0 in both the electron-diffraction structure and in a structure in which the x-ray structure is overlaid on the double-membrane configuration. These portals are large enough to allow the access of intercellular water molecules to the extracellular vestibule of all channels.

What are the forces that are involved in stabilizing the close association of the extracellular domains of AQP0 as seen in the electron-diffraction structure or in the x-ray structure superposed on the double-membrane? Analysis of both structures shows that there are no direct hydrogen bonds between adjacent extracellular domains. The primary interactions between extracellular domains are hydrophobic contacts (Fig. 4 *Lower Right*).

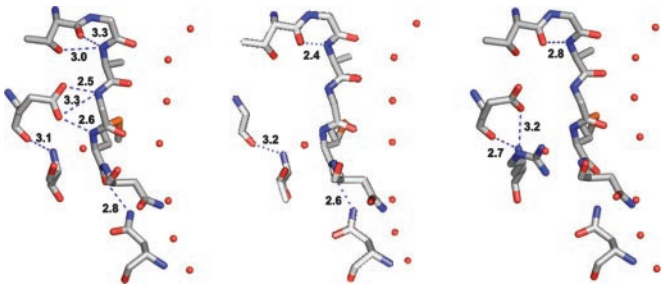

Fig. 5. Diagrams of the region surrounding the E134G and T138R cataract mutations. Overall, bovine and human amino acid sequences share 94% identity, and with regard to the amino acids shown in Fig. 6, all are conserved. Therefore, parallels can be made regarding their effect on channel permeability. The figures were produced with MOLOC and the mutation structure underwent minimization by using the molecular mechanics force field of CNS. Possible hydrogen-bonding pairs are connected by yellow dotted lines.

Congenital Mutations of AQP0 That Induce Cataracts. Certain human congenital cataracts are the result of either of the following two independent single amino acid-substitution mutations in the AQP0 molecule: Glu134Gly or Thr138Arg (31). These residues, conserved in essentially all AQPs, are located in the middle of the M5 helix and are buried relative to the surface of the molecule. Glu-134 hydrogen bonds to successive peptide NHs and orients the line of four backbone carbonyls (Gly-180, Ala-181, and Gly-182, and Met-183) that provide the hydrogen bond acceptors for adjacent channel waters in the channel (Fig. 5 *Left*). Thus, Glu134Gly would remove this orienting factor and distort the line of carbonyls, altering the conductance for water (Fig. 5 *Center*). Thr-138 is very close to Glu-134 and may also distort this region of the channel (Fig. 5 *Right*). The Thr138Arg mutation removes the interaction with Glu-134 and replaces it with a bulky side chain in the midmembrane domain, again distorting the line of functional carbonyls in the channel (Fig. 5).

bAQP0 and Cell–Cell Adhesion. Immunocytochemical labeling and freeze-fracture experiments localized AQP0 to the flat junctional plaques as well as to the characteristic "ball-and-socket" and "tongue-and-groove" interdigitations of the vertebrate lens. Freeze-fracture experiments showed no evidence of coaxial AQP0-to-AQP0 opposition; bumps on one membrane always aligned with a corresponding depression on the other membrane (32). With this evidence, it appears that bAQP0 does not form typical gap-junction structures where hemiconnexons form direct coaxial channels from the cytoplasm of one cell to the cytoplasm of an adjacent cell. This evidence does not rule out a cell-to-cell transport role for AQP0, although both extracellular vestibules are accessible to the intercellular space.

The localization of AQP0 into junction-like plaques, especially those forming curved membrane structures, leads to the postulate that AQP0 contacts are involved in cell-to-cell adhesion and/or the generation of curved membrane structures (37). In addition, phosphatidylcholine based proteoliposomes preferentially associate with phosphatidylserine vesicles only when AQP0 was present, suggesting a charged interaction (35, 38). Counting charged amino acid side chains in the extracellular surface of the bAQP0 shows the surface to be net +4 positively charged per monomer and +16 per tetramer at physiological pH. This observation helps to explain the observed association between the extracellular domain of AQP0 and large unilamellar liposomes constructed exclusively of negatively charged phosphatidylserine. With each opposing surface having a net positive charge of +16, the tetramers would tend to repel each other without the hydrophobic interactions that we see dominating the other type of junctional AQP0–AQP0 contacts.

The roles of AQP0 as a water transporter and cell-adhesion molecule dovetail well with the cell biology of the lens. The water transport function of AQP0 aids the maintenance of water homeostasis and osmotic balance in the lens. The cell-adhesion role of AQP0 supports the structure and function of the lens by providing mechanical bonding of adjacent fiber cells, allowing them to resist the strain of optical accommodation during focusing and to minimize light scatter by keeping intercellular spaces small. The adhesion between the extracellular surface of AQP0 and the negatively charged portion of the membrane could also augment the structural strength of the lens as a whole and act to minimize extracellular spaces that would otherwise generate excessive light scatter.

We thank the staff of Beamline 8.3.1 at the Advanced Light Source (ALS) at the Lawrence Berkeley National Laboratory, and Dr. Christopher Waddling (University of California, San Francisco) for x-ray support. This work was supported by National Institutes of Heath Grant GM24485 (to R.M.S.).

1. Kinoshita, J. H., Kador, P. & Catiles, M. (1981) *J. Am. Med. Assoc.* **246,** 257–261.
2. Trokel, S. (1962) *Invest. Ophthalmol.* **1,** 493–501.
3. Kinoshita, J. H. & Merola, L. O. (1964) *Invest. Ophthalmol.* **47,** 577–584.
4. Bloemendal, H. (1977) *Science* **197,** 127–138.
5. Rink, H. (1982) *Biophys. Struct. Mech.* **9,** 95–101.
6. Lasser, A. & Balazs, E. A. (1972) *Exp. Eye Res.* **13,** 292–308.
7. Wistow, G. J., Pisano, M. M. & Chepelinsky, A. B. (1991) *Trends Biochem. Sci.* **16,** 170–171.
8. Park, J. H. & Saier, M. H., Jr. (1996) *J. Membr. Biol.* **153,** 171–180.
9. Sui, H., Han, B. G., Lee, J. K., Walian, P. & Jap, B. K. (2001) *Nature* **414,** 872–878.
10. Gonen, T., Sliz, P., Kistler, J., Cheng, Y. & Walz, T. (2004) *Nature* **429,** 193–197.
11. Nemeth-Cahalan, K. L. & Hall, J. E. (2000) *J. Biol. Chem.* **275,** 6777–6782.
12. Nemeth-Cahalan, K. L., Kalman, K. & Hall, J. E. (2004) *J. Gen. Physiol.* **123,** 573–580.
13. Virkki, L. V., Cooper, G. J. & Boron, W. F. (2001) *Am. J. Physiol.* **281,** R1994–R2003.
14. Shen, L., Shrager, P., Girsch, S. J., Donaldson, P. J. & Peracchia, C. (1991) *J. Membr. Biol.* **124,** 21–32.
15. Bloemendal, H., Bont, W. S., Jongkind, J. F. & Wisse, J. H. (1962) *Nature* **193,** 437–439.
16. Konig, N., Zampighi, G. A. & Butler, P. J. (1997) *J. Mol. Biol.* **265,** 590–602.
17. Aerts, T., Xia, J. Z., Slegers, H., de Block, J. & Clauwaert, J. (1990) *J. Biol. Chem.* **265,** 8675–8680.
18. Otwinowski, Z. & Minor, W. (1997) in *Methods in Enzymology*, eds. Carter, C. W., Jr., & Sweet, R. M. (Academic, New York), Vol. 276, pp. 307–326.
19. Leslie, A. G. W. (1992) *Joint CCP4 ESF–EAMCB Newslett. Prot. Crystallogr.* **26**.
20. Brunger, A. T. (1998) *Acta Crystallogr. D* **54,** 905–921.
21. Gerber, P. R., Muller, K. (1995) *J. Comput. Aided Mol. Des.* **9,** 251–268.
22. Savage, D. F., Egea, P. F., Robles-Colmenares, Y., O'Connell, J. D. & Stroud, R. M. (2003) *PLoS Biol.* **1,** 334–340.
23. Fu, D., Libson, A., Miercke, L. J., Weitzman, C., Nollert, P. & Stroud, R. M. (2000) *Science* **290,** 481–486.
24. Chandy, G., Zampighi, G. A., Kreman, M. & Hall, J. E. (1997) *J. Membr. Biol.* **159,** 29–39.
25. Mulders, S. M., Preston, G. M., Deen, P. M., Guggino, W. B., van Os, C. H. & Agre, P. (1995) *J. Biol. Chem.* **270,** 9010–9016.
26. Yang, B. & Verkman, A. S. (1997) *J. Biol. Chem.* **272,** 16140–16146.
27. Varadaraj, K., Kushmerick, C., Baldo, G. J., Bassnett, S., Shiels, A. & Mathias, R. T. (1999) *J. Membr. Biol.* **170,** 191–203.
28. Kushmerick, C., Rice, S. J., Baldo, G. J., Haspel, H. C. & Mathias, R. T. (1995) *Exp. Eye Res.* **61,** 351–362.
29. Kushmerick, C., Varadaraj, K. & Mathias, R. T. (1998) *J. Membr. Biol.* **161,** 9–19.
30. Lampe, P. D., Bazzi, M. D., Nelsestuen, G. L. & Johnson, R. G. (1986) *Eur. J. Biochem.* **156,** 351–357.
31. Francis, P., Chung, J. J., Yasui, M., Berry, V., Moore, A., Wyatt, M. K., Wistow, G., Bhattacharya, S. S. & Agre, P. (2000) *Hum. Mol. Genet.* **9,** 2329–2334.
32. Costello, M. J., McIntosh, T. J. & Robertson, J. D. (1985) *Curr. Eye Res.* **4,** 1183–1201.
33. Costello, M. J. & Fetter, R. D. (1986) *Methods Enzymol.* **127,** 704–718.
34. Costello, M. J., McIntosh, T. J. & Robertson, J. D. (1989) *Invest. Ophthalmol. Vis. Sci.* **30,** 975–989.
35. Michea, L. F., Andrinolo, D., Ceppi, H. & Lagos, N. (1995) *Exp. Eye Res.* **61,** 293–301.
36. Stroud, R. M. & Fauman, E. B. (1995) *Protein Sci.* **4,** 2392–2404.
37. Zampighi, G. A., Hall, J. E., Ehring, G. R. & Simon, S. A. (1989) *J. Cell Biol.* **108,** 2255–2275.
38. Michea, L. F., de la Fuente, M. & Lagos, N. (1994) *Biochemistry* **33,** 7663–7669.
39. Smart, O. S., Neduvelil, J. G., Wang, X., Wallace, B. A. & Sansom, M. S. P. (1996) *J. Mol. Graphics* **14,** 354–360.